

**ITERATIVE AND SINGLE-STEP SOLUTIONS OF TWO  
DIMENSIONAL TIME-DOMAIN INVERSE SCATTERING PROBLEM  
FEATURING ULTRA WIDE BAND SENSORS**

**SAEED ALI SAEED BINAJJAJ**

**UNIVERSITI SAINS MALAYSIA  
2010**

**ITERATIVE AND SINGLE-STEP SOLUTIONS OF  
TWO DIMENSIONAL TIME-DOMAIN INVERSE SCATTERING  
PROBLEM FEATURING ULTRA WIDE BAND SENSORS**

**by**

**SAEED ALI SAEED BINAJJAJ**

**Thesis submitted in fulfillment of the  
requirements for the degree of  
Doctor of Philosophy**

**June 2010**

## **DEDICATION**

To...

My uncle, mother, wife and wonderful kids

My brothers, sisters and their kids

My supervisor for his efforts

My friends with respect

I dedicate this work ...

## **ACKNOWLEDGEMENTS**

First of all, thanks to ALLAH for completing and finishing this research work .I would like to express special acknowledgement to my supervisor, Professor Dr. Mohd Zaid Abdullah in terms of deepest gratitude for his invaluable suggestion, support, constructive criticisms and comments as well as fruitful discussions that have remarkably influenced this research work and without which I would not have succeeded in carrying out this research. I am proud to work under his supervision in the research.

I would like also to express my deep gratitude to my family for their continuous support and encouragement as well as unlimited patience with me during the years of this research, especially my mother, which bore the separation, as well as my wife, who bore the alienation and distance from the family and did not complain and was supportive of me.

I would like also to thank my colleagues Tareq Zanoon, Hanif, Saad, Motasem, who provided me with help and encouragement in this research. Furthermore, I can't forget the unknown soldiers, Mr. Amer and Mr. Azhar, lab technicians, and I would like to record special words of thanks for their invaluable cooperation and friendly attitude.

Last but not least I would like to express my sincere thanks to all the staff at the School of Electrical and Electronic Engineering, University Sains Malaysia, as well as for school itself for their cooperation and providing us with the necessary facilities for

this research. Also, I acknowledge receiving financial support from USM under The Research University Grant Scheme (1001.PELECT.814012).

## TABLE OF CONTENTS

	Page
<b>DEDICATION.....</b>	<b>i</b>
<b>ACKNOWLEDGEMENTS.....</b>	<b>iv</b>
<b>TABLE OF CONTENTS.....</b>	<b>vi</b>
<b>LIST OF TABLES .....</b>	<b>xi</b>
<b>LIST OF FIGURES .....</b>	<b>xii</b>
<b>LIST OF ABBREVIATIONS .....</b>	<b>xix</b>
<b>LIST OF SYMBLOS .....</b>	<b>xxi</b>
<b>ABSTRAK .....</b>	<b>xxiii</b>
<b>ABSTRACT.....</b>	<b>xxv</b>
<b>CHAPTER 1 - INTRODUCTION .....</b>	<b>1</b>
1.1 Introduction.....	1
1.2 Inverse Electromagnetic Scattering.....	3
1.2.1 Mathematical Challenges .....	4
1.2.1.1 Electromagnetic Scattering .....	4
1.2.1.2 Non-linearity .....	4
1.2.1.3 Ill-Posedness .....	5
1.2.2 Application of Electromagnetic Inverse Problem.....	5
1.2.2.1 Military Applications .....	6
1.2.2.2 Medical Applications .....	7
1.2.2.3 Industrial Applications.....	8
1.2.2.4 Scientific Applications .....	9

1.2.3	Development of Inversion Algorithms .....	10
1.2.3.1	Linearized Inversion Algorithms .....	11
1.2.3.2	Non-linear Inversion Algorithms .....	11
1.3	Thesis Objectives .....	13
1.3.1	General Objective.....	13
1.3.2	Specific Objectives.....	13
1.4	Thesis Outlines.....	14
<b>CHAPTER 2 - LITERATURE REVIEW.....</b>		<b>16</b>
2.1	Introduction.....	16
2.2	Tomography History .....	16
2.2.1	Computed Tomography .....	17
2.2.2	Ultrasound Tomography .....	19
2.3	Soft Field vs. Hard Field Systems.....	22
2.4	Non-Diffraction Tomography .....	24
2.5	Diffraction Tomography .....	36
2.5.1	The First Born Approximation.....	40
2.5.2	Plane Wave Approach.....	40
2.6	Non-linear Inverse Scattering .....	47
2.6.1	Frequency Domain Methods .....	48
2.6.2	Time-Domain Methods .....	49
2.6.3	Optimization Process .....	52
2.6.3.1	Global Inversion Algorithms.....	52
2.6.3.2	Local Inversion Algorithms .....	53
2.6.4	Proposed Algorithm .....	54

<b>CHAPTER 3 - PROBLEM FORMULATION.....</b>	<b>55</b>
3.1 Introduction.....	55
3.2 Problem Definition.....	56
3.3 Problem Description .....	56
3.3.1 TM Mode System.....	58
3.4 Mathematical Minimization Process.....	59
3.4.1 Direct Problem .....	63
3.4.2 Adjoint Problem.....	63
3.4.3 Gradient of the Cost Function .....	68
3.5 Local Optimization Methods.....	69
3.5.1 Second Order Methods.....	70
3.5.1.1 Newton’s Method.....	70
3.5.1.2 Quasi Newton’s Method .....	72
3.5.2 First Order Methods .....	73
3.5.2.1 Steepest Descent .....	74
3.5.2.2 Conjugate Gradient .....	77
3.5.2.2.1 Linear Conjugate Gradient.....	78
3.5.2.2.2 Non-linear Conjugate Gradient.....	81
3.5.3 Iterative Inversion Algorithm.....	86
3.5.4 Single-Step Inversion Algorithm .....	89
3.5.5 Reconstruction Errors .....	92
<b>CHAPTER 4 - METHOD AND MATERIALS .....</b>	<b>94</b>
4.1 Introduction.....	94
4.2 Software Implementation (FDTD Method) .....	95



4.2.1	Discretization Used in FDTD Method .....	96
4.2.1.1	Discretization of 1-D Maxwell's Equations.....	96
4.2.1.1.1	EM Propagation in Free Space.....	99
4.2.1.1.2	Mur's Absorbing Boundary Conditions.....	101
4.2.1.1.3	EM Propagation in Dielectric and Lossy Medium... .....	108
4.2.1.2	Cell Size and Numerical Dispersion .....	112
4.2.1.3	Courant Stability .....	113
4.2.1.4	Discretization of 2-D Maxwell's Equations.....	114
4.2.1.4.1	Perfectly Matched Layer (PML).....	122
4.2.2	Inverse Scattering Problem Discretization.....	132
4.2.2.1	Forward Problem Discretization .....	133
4.2.2.2	Adjoint Problem Discretization .....	139
4.2.2.3	Gradient Discretization .....	144
4.3	Hardware Implementation (Experimental Setup) .....	144
4.3.1	Data Acquisition Systems .....	145
4.3.1.1	UWB Sensors .....	145
4.3.1.2	Vector Network Analyzer .....	146
4.3.2	Limited View Scanning Geometry .....	147
4.3.3	Full View Scanning Geometry.....	148
<b>CHAPTER 5 - RESULTS AND DISCUSSIONS .....</b>		<b>150</b>
5.1	Introduction.....	150
5.2	Limited View Scanning Geometry .....	150
5.2.1	Simulation Results .....	152

5.2.2	Experimental Results .....	160
5.3	Full View Geometry.....	166
5.3.1	Simulation Results .....	167
5.3.2	Experimental Results .....	177
5.4	Accuracy and reliability Assessment .....	181
5.4.1	Shape of the Excitation Signal.....	182
5.4.2	Bandwidth of the Excitation Signal .....	185
5.4.3	Absorbing Boundary Conditions .....	189
5.5	Observations.....	199
<b>CHAPTER 6 - CONCLUSION AND FUTURE WORK.....</b>		<b>202</b>
6.1	Conclusions.....	202
6.2	Suggestions for future work.....	206
6.2.1	Modeling of Electromagnetic Waves.....	206
6.2.2	The Modeling of Curved Objects.....	207
6.2.3	Measurement Error Minimization.....	208
<b>REFERENCES .....</b>		<b>209</b>
<b>APPENDICES .....</b>		<b>222</b>
APPENDIX A .....		222
APPENDIX B .....		226
<b>LIST OF PUBLICATIONS.....</b>		<b>228</b>

## LIST OF TABLES

	Page
Table 5.1	Simulation results employing limited view scanning geometry .....153
Table 5.2	Results summarizing the laboratory experiments employing limited view scanning geometry.....161
Table 5.3	Simulation results employing full view scanning geometry.....168
Table 5.4	Results summarizing the laboratory experiments employing full view scanning geometry. ....177
Table 5.5	Summary observation and comparison between the current research with recent published works related to the inverse scattering probl ...201

## LIST OF FIGURES

		Page
Figure 1.1	Latest system for land mines detection (Wampler, 2009).....	7
Figure 1.2	Shows the CAT machine commonly used by hospitals (IMAGING, 2009) .....	8
Figure 1.3	Capacitance type of process tomography flow sensor (Hoyle, 2009).....	9
Figure 1.4	X-ray Diffraction Equipment Used in Scientific Applications (EQUIPMENT, 2009).....	10
Figure 2.1	The object and its projection $P_{\theta}(t)$ taken at an angle $\theta$ .....	26
Figure 2.2	Types of projection (a) the parallel projections and (b) fan beam projection which used in the scheme of the CT scanner for different generations .....	27
Figure 2.3	The relation between 1-D Fourier transform of the projection and the 2-D Fourier transform of the object along the radial line BB- the graphic meaning of the Fourier Slice Theorem.....	30
Figure 2.4	Frequency domain representation of the projections (a) radial grid and (b) square grid .....	31
Figure 2.5	Typical diffraction experiment.....	38
Figure 2.6	Fourier Diffraction Theorem.....	44
Figure 3.1	FDTD grid used to model the propagation of TM's wave in (a) cross-hole geometry, and (b) full angle view geometry. The grid is truncated by first and second order Mur absorbing boundary conditions.....	57
Figure 3.2	Overall descriptions of the iterative inversion algorithm.....	89
Figure 3.3	Overall description of the single-step algorithm.....	92
Figure 4.1	Discretization procedure followed by FDTD scheme.....	98
Figure 4.2	1-D FDTD simulation of the Gaussian pulse propagates in the free space .....	100
Figure 4.3	1-D FDTD grid at the boundary $x=0$ and the way at which the spatial and time derivative are approximated.....	105

Figure 4.4	Four snap shoots of 1-D FDTD simulation describing the effect of using the first order Mur's ABC to eliminate the reflection ..... 107
Figure 4.5	Four snap shots of FDTD simulation describing the behavior of the pulse strikes the dielectric medium. The source originates at cell number (5)..... 109
Figure 4.6	Three snapshots of FDTD simulation describing the pulse when hitting the lossy dielectric medium..... 111
Figure 4.7	FDTD grid for TM mode Maxwell's equation ..... 115
Figure 4.8	2-D representation of free space 2-D FDTD simulation for four snapshots (a), (b), (c) and (d) taken at time steps 40, 60, 80 and 180 corresponding to 67, 100, 133 and 300 ps respectively ..... 116
Figure 4.9	3-D representation of free space 2-D FDTD simulation for four snapshots (a), (b), (c) and (d) taken at time steps 40, 60, 80 and 180 corresponding to 67, 100, 133 and 300 ps respectively ..... 117
Figure 4.10	2-D FDTD grid truncated by Mur ABCs..... 118
Figure 4.11	2-D representation of free space 2-D FDTD simulation truncated by Mur's ABC for four snapshots (a), (b), (c) and (d) taken at time steps 40, 60, 80 and 180 corresponding to 67, 100, 133 and 300 ps respectively .. ..... 120
Figure 4.12	3-D representation of free space 2-D FDTD simulation truncated by Mur's ABC for four snapshots (a), (b), (c) and (d) taken at time steps 40, 60, 80 and 180 corresponding to 67, 100, 133 and 300 ps respectively .. ..... 121
Figure 4.13	Structure of 2-D FDTD grid using PML ABC. .... 126
Figure 4.14	2-D representation of free space 2-D FDTD simulation truncated by PML ABC for four snapshots (a), (b), (c) and (d) taken at time steps 40, 60, 80 and 180 corresponding to 67, 100, 133 and 300 ps respectively .. ..... 129
Figure 4.15	3-D representation of free space 2-D FDTD simulation truncated by PML ABC for four snapshots (a), (b), (c) and (d) taken at time steps 40, 60, 80 and 180 corresponding to 67, 100, 133 and 300 ps respectively .. ..... 130
Figure 4.16	1-D representation for two 2-D FDTD simulations: a and b belongs to the first FDTD truncated by Mur's ABC, c and d belongs to the second truncated by PML..... 131

Figure 4.17	1-D representation for two 2-D FDTD simulations where only the cells near the boundary are illustrated.....	132
Figure 4.18	Forward problem employing limited view scanning geometry implementation when excited from the tenth transmitter illustrated by four snapshots (a), (b), (c) and (d) taken at time steps 100, 150, 250 and 350 corresponding to 1.67, 2.5, 4.17 and 5.83 ns respectively .....	136
Figure 4.19	Measurement Process employing limited view scanning geometry implementation when excited from the tenth transmitter illustrated by four snapshots (a), (b), (c) and (d) taken at time steps 100, 150, 250 and 350 corresponding to 1.67, 2.5, 4.17 and 5.83 ns respectively .....	137
Figure 4.20	Forward problem employing full view scanning geometry implementation when excited from the transceiver with yellow color illustrated by four snapshots (a), (b), (c) and (d) taken at time steps 100, 120, 170 and 250 corresponding to 1.67, 2, 2.83 and 4.17 ns respectively .....	138
Figure 4.21	Measurement process employing full view scanning geometry implementation when excited from the transceiver with yellow color illustrated by four snapshots (a), (b), (c) and (d) taken at time steps 100, 120, 170 and 250 corresponding to 1.67, 2, 2.83 and 4.17 ns respectively .....	139
Figure 4.22	Adjoint problem employing limited view scanning geometry implementation when excited from the all receivers illustrated by four snapshots (a), (b), (c) and (d) taken at time steps 20, 50, 120 and 170 corresponding to 0.33, 0.83, 2 and 2.83 ns respectively .....	142
Figure 4.23	Adjoint problem employing limited view scanning geometry implementation when excited from the all transceivers except one used by forward problem, illustrated by four snapshots (a), (b), (c) and (d) taken at time steps 20, 120, 150 and 170 corresponding to 0.33, 2, 2.5, and 2.83 ns respectively.....	143
Figure 4.24	UWB antenna showing (a) schematic, (b) actual antenna with ferrite core .....	146
Figure 4.25	Experimental set-up for UWB limited view geometry, (a) the schematic, (b) the essential elements .....	148
Figure 4.26	The experimental set-up for UWB tomography full view geometry, (a) the schematic and (b) the essential elements.....	149

Figure 5.1	Example of excitation signals assumed in the limited view reconstruction, (a) modulated cosine Gaussian with 1 GHz central frequency, (b) its spectrum, and (c) is the derivative of (a) “red” and sample of homogenous experimental data “black “ ..... 152
Figure 5.2	Simulation results for one object at center, (a) actual image, (b) reconstructed image using single-step and (c) reconstructed image using iterative algorithm ..... 155
Figure 5.3	3-D representation of Figure 5.2, (a) actual profile, (b) reconstructed profile after 16 iterations and (c) the convergence trend ..... 156
Figure 5.4	Reconstruction errors of Figure 5.2, (a) contour plot, (b) and (c) are pixel and image reconstruction errors respectively ..... 157
Figure 5.5	Simulation result for two objects, (a) actual image (b) reconstructed image using single-step, and (c) reconstructed image using iterative algorithm ..... 158
Figure 5.6	3-D representation of Figure 5.5, (a) actual profile, (b) reconstructed profile after 16 iterations, and (c) the convergence trend ..... 159
Figure 5.7	Reconstruction errors of Figure 5.5, (a) contour plot, (b) and (c) are pixel and image reconstruction errors respectively ..... 160
Figure 5.8	The difference between homogenous simulation data “blue“ and homogenous experimental data “red“ for same transceiver pairs after time alignment and amplitude normalization ..... 163
Figure 5.9	Calibration of the imaging instrument showing the waveform pattern obtained from one projection, (a) the simulated pulse, (b) the measured pulse and (c) the calibrated pulse ..... 164
Figure 5.10	Image reconstruction of a pumpkin located at the center, (a) actual, (b) reconstructed before smoothing and (c) reconstructed after smoothing ..... 165
Figure 5.11	Image reconstruction of two plastic phantoms of different sizes and shapes, (a) actual, (b) reconstructed before smoothing and (c) reconstructed after smoothing ..... 166
Figure 5.12	Example of excitation signals assumed in the full view reconstruction, (a) measured signal “red” and simulated Gaussian with 2 GHz band width “blue”, and (b) their spectrum ..... 167

Figure 5.13	Simulation results for one object at center, (a) actual image, (b) reconstructed image using single-step and (c) reconstructed image using iterative algorithm ..... 172
Figure 5.14	A 3-D representation of Figure 5.13, (a) actual profile, (b) reconstructed profile after 59 iterations and (c) the convergence trend ..... 172
Figure 5.15	Reconstruction errors of Figure 5.13, (a) contour plot, (b) and (c) are pixel and image reconstruction errors respectively ..... 173
Figure 5.16	Simulation result for two objects, (a) actual image, (b) reconstructed image using single-step and (c) reconstructed image using iterative algorithm ..... 173
Figure 5.17	A 3-D representation of Figure 5.16, (a) actual profile, (b) reconstructed profile after 59 iterations and (c) the convergence trend ..... 174
Figure 5.18	Reconstruction errors of Figure 5.16, (a) contour plot, (b) and (c) are pixel and image reconstruction errors respectively ..... 175
Figure 5.19	Simulation result for Z letter object, (a) actual image, (b) reconstructed image using single-step and (c) reconstructed image using iterative algorithm ..... 175
Figure 5.20	3-D representation of Figure 5.19, (a) actual profile, (b) reconstructed profile after 59 iterations and (c) the convergence trend ..... 176
Figure 5.21	Reconstruction errors of Figure 5.19, (a) contour plot, (b) and (c) are pixel and image reconstruction errors respectively ..... 176
Figure 5.22	The difference between full view homogenous simulation data “blue“ and homogenous experimental data “red“ for same transceiver pairs after time alignment and amplitude normalization ..... 179
Figure 5.23	Calibration of the imaging instrument showing the waveform pattern obtained from one projection, (a) the simulated pulse, (b) the measured pulse and (c) the calibrated pulse ..... 180
Figure 5.24	Image reconstruction of full view experiments, (a) actual egg, (b) location and (c) reconstructed ..... 181
Figure 5.25	Image reconstruction of full view experiments, (a) actual carrot, (b) location and (c) reconstructed ..... 181



Figure 5.26	Image reconstruction of letter Z object using different pulses, (a) actual image, (b) and (d) are the single-step and iterative reconstruction using Gaussian pulse respectively, and (c) and (d) are same as (b) and (d) but using modulated Gaussian.....	184
Figure 5.27	Reconstruction errors of iterative algorithm in Figure 5.26 where (a) and (b) are the image reconstruction errors using Gaussian and modulated Gaussian respectively, and (c) and (d) are their corresponding contour plots vs. the contour of actual profile.....	185
Figure 5.28	The single-step reconstruction of letter Z object using modulated Gaussian pulse with different bandwidths, (a) actual image, (b), (c) and (d) are the reconstructed images using 1GHz, 2 GHz and 3 GHz respectively .....	187
Figure 5.29	The iterative reconstruction of letter Z object using modulated Gaussian pulse with different bandwidths, (a) actual image , (b), (c) and (d) are the reconstructed images using 1 GHz, 2 GHz and 3 GHz respectively .....	188
Figure 5.30	Reconstruction errors of iterative algorithm in Figure 5.29 where (a), (b) and (c) are the image reconstruction errors using three modulated Gaussian pulses with bandwidths 1,2,6 GHz respectively and (c) (d) and (e) are their corresponding contour plots vs. the contour of actual profile	189
Figure 5.31	The single-step reconstruction of letter Z object using different ABCs, (a) actual image, (b) and (c) are the reconstructed images using Mur and PML ABCs respectively.....	191
Figure 5.32	The iterative reconstruction of letter Z object using different ABCs, (a) actual image, (b) and (c) are the reconstructed images using Mur and PML ABCs respectively.....	191
Figure 5.33	Reconstruction errors of iterative algorithm in Figure 5.32 where (a), and (b) are the image reconstruction errors using Mur's and PML ABCs respectively, (c) and (d) are the actual contours superimposed with the reconstruction contours in (a) and (b) respectively.....	192
Figure 5.34	Computational domain and the grid cells required to employ, (a) PML ABC, and (b) Mur's ABCs for the truncation purpose .....	194
Figure 5.35	Contour plot of the actual profile for letter Z object.....	195
Figure 5.36	Contour plot of reconstructed image obtained by modulated Gaussian with 6 GHz bandwidth .....	196

Figure 5.37 Shows noisy simulated data with average signal to noise ratio, (a) 9dB and (b) 6dB where these samples are taken from 1-2, 1-3, 1-4 and 1-5 transceiver pairs from top to bottom respectively ..... 198

Figure 5.38 Single-step reconstructions produced from noise free and noisy data: (a) and (d) are results of noise free data, (b) and (e) are results with 9 dB SNR, and (c) and (f) results with 6 dB SNR ..... 198

Figure 5.39 Iterative reconstructions produced from noise free and noisy data: (a) and (d) are results of noise free data , (b) and (e) are results with 9 dB SNR, and (c) and (f) results with 6 dB SNR ..... 199

## LIST OF ABBREVIATIONS

1-D , 2-D and 3-D	One , Two And Three Dimensional
ABCs	Absorbing Boundary Conditions
ART	Algebraic Reconstruction Technique
BC	Boundary Conditions
BIM	Born Iterative Method
CGM	Conjugate Gradient Method
CT	Computed Tomography
DBIM	Distorted Born Iterative Method
EM	Electromagnetic
FDTD	Finite Difference Time-Domain Method
FEM	Finite Element Method
IC	Initial Conditions
LMM	Levenberg-Margurdt Method
MOM	Method of Moments
NKM	Newton Kantorovich Method
PML	Perfectly Matched Layer
SART	Simultaneous Algebraic Reconstruction Technique
SIRT	Simultaneous Iterative Reconstruction Technique
SNR	Signal to Noise Ratio
T/R	Transceiver
TE	Transverse Electric

TM Transverse Magnetic

UWB Ultra Wide Band

## LIST OF SYMBLOS

$c$	Phase Velocity
$c_0$	Free Space Phase Velocity
$E$	Electric Field
$e$	Adjoint Electric Field
$g$	Gradient
$H$	Magnetic Field
$h$	Adjoint Magnetic Field
$H$	Hessian Matrix
$i$	Index Number Along X Axis
$j$	Index Number Along Y Axis
$J$	TM Short Pulse
$k^*$	Complex Wave Number
$k_0$	Wave Number
$L$	Total Number of Pixels
$M$	Total Number of Receivers
$N$	Total Number of Transmitters
$n$	Number of Forward Time Step
$n^*$	Number of Backward Time Step
$Nt$	Total Number of Time Steps
$Nx$	Total Number of Indices Along X Axis
$Ny$	Total Number of Indices Along Y Axis
$t$	Forward Time

$T$	Total Scanning Time
$u$	Spatial Frequency along u
$v$	Spatial Frequency along v
$\alpha$	Real Part of Propagation Constant
$\beta$	Imaginary Part of Propagation Constant
$\delta(.)$	Dirac Delta Function
$\varepsilon$	Permittivity
$\varepsilon_0$	Free Space Permittivity
$\varepsilon_r$	Relative Permittivity
$\eta$	Characteristic Impedance
$\eta_0$	Characteristic Impedance of Free Space
$\theta$	View Angle
$\lambda$	Wave Length
$\mu$	Permeability
$\mu_0$	Free Space Permeability
$\mu_r$	Relative permeability
$\nu$	Regularization Parameter
$\sigma$	Electric Conductivity
$\sigma^*$	Magnetic Conductivity
$\tau$	Backward Time
$\omega$	Angular Frequency
$\omega^*$	Complex Angular Frequency
$\Gamma$	2-D Spatial Domain

**PENYELESAIAN BERLELAR DAN SELANGKAH BAGI MASALAH  
PENYERAKAN SONGSANG DOMAIN-MASA DUA DIMENSI  
MENGEMUKAKAN SENSOR ULTRA BERJALUR LEBAR**

**ABSTRAK**

Kajian ini membincangkan tomografi penyerakan songsang domain masa ultra jalur lebar (UWB) yang digunakan untuk membina semula ciri-ciri dielektrik sasaran yang tidak diketahui dalam 2D. Algoritma pembinaan semula imej berdasarkan kepada peminimuman kecerunan kos fungsi luasan yang didefinisikan sebagai perbezaan antara medan yang diukur dan yang dikira. Pengiraan fungsi kepekaan ini memerlukan dua langkah berturut-turut: perambatan ke hadapan (langsung) medan-gelombang UWB, (ii) perambatan terbalik (dampungan) gelombang-gelombang sisa. Gelombang langsung dan dampungan dikira menggunakan kaedah perbezaan terhingga domain masa (FDTD), dengan melaksanakan syarat-syarat peyerapan sempadan Mur dan lapisan terpadan sempurna (PML). Algoritma pengimejan adalah berasaskan kepada teknik pengoptimuman yang tak linear, dan daripada ini, sekema songsang berlelar atau satu langkah direalisasikan. Pertamanya, perlakuan algoritma-algoritma ini diselidiki melalui simulasi berangka menggunakan dua geometri pengimbasan yang berbeza: geometri pengimbasan pengelihatan terhad dan pengelihatan penuh di mana kebolegunaan algoritma dinilai dengan membandingkan imej-imej dibina semula dengan model sebenar. Keduanya, masalah kestabilan serta syarat-syarat pengiraan disiasat menggunakan empat data eksperimen yang diukur oleh dua sistem perolehan data yang berbeza. Dalam eksperimen ini juga, objek-objek organik dengan ciri-ciri yang pelbagai telah digunakan untuk mensimulasi profil dielektrik tisu-tisu kanser, manakala paip

plastik digunakan untuk pengujian perlakuan yang lebih mendalam. Sementara itu lagi, ketahanan algoritma terhadap data hingar dinilai menggunakan dua simulasi eksperimen dengan nisbah isyarat-ke-bising 6 dan 8dB, masing-masingnya. Keputusan menunjukkan algoritma berkeupayaan untuk menghuraikan profil dielektrik yang agak rumit dengan resolusi mendekati skala milimeter meskipun dengan kehadiran hingar yang tinggi. Keputusan juga menunjukkan algoritma mampu menghuraikan ciri-ciri objek yang bersaiz setanding setengah jarak gelombang untuk data penyerakan yang diukur dari sudut pandangan terhad. Algoritma langkah tunggal menunjukkan ketahanan terhadap hingar lebih daripada algoritma berlelar walaupun dengan penggunaan regularisasi. Namun, kaedah berlelar lebih tepat apabila membina semula imej tanpa hingar berbanding dengan teknik langkah tunggal. Dalam semua kes, algoritma berlelar mencapai ketepatan yang lebih baik dari 90% dan 98% untuk data pengelihatan terhad dan penuh masing-masingnya



**ITERATIVE AND SINGLE-STEP SOLUTIONS OF TWO  
DIMENSIONAL TIME-DOMAIN INVERSE SCATTERING PROBLEM  
FEATURING ULTRA WIDE BAND SENSORS**

**ABSTRACT**

This study investigates the time-domain inverse scattering of ultra wide band (UWB) tomography used in reconstructing the dielectric properties of the unknown targets in two dimensions. The image reconstruction algorithm was based on the gradient minimization of an augmented cost function defined as the difference between measured and calculated fields. Computation of the sensitivity function required two successive steps: (i) the forward (direct) propagation of the UWB wave-field, and (ii) the reverse (adjoint) propagation of the residual waves. The direct and adjoint fields were calculated using the finite-difference time-domain (FDTD) method, implementing the Mur's and the perfectly matched layer (PML) absorbing boundary conditions. The imaging algorithm was based on a non-linear optimization technique from which the single-step and iterative inversion schemes were realized. First, the algorithms' performances were evaluated using numerical simulation employing two different scanning geometries: limited and full view scanning geometries, where the applicability of these algorithms was accessed by comparing the reconstructed images with actual model. Second, the stability problem and the computational requirements were investigated using four experimental data collected by two different data acquisition systems. In experiments, organic objects with various properties were used to simulate cancerous-like dielectric profile, while the plastic pipe was employed for further performance and testing purposes. Finally, the algorithms' robustness against the noisy data was evaluated using two simulated experiments with signal-to-noise ratios of 6 and 8 dB respectively.

Results indicate that fairly complicated dielectric profiles can be accurately reconstructed at near millimeter resolution even with the presence of high noise levels. In addition, the algorithms were able to resolve features which sizes that are comparable to the half wave-length for scattered data collected from limited as well as full view angles. The single-step algorithm showed robustness against the noise more than the iterative algorithm even when regularization method was used. However, the iterative technique is more accurate in reconstructed noise free images compared to the single-step method. In all cases, the iterative algorithm attained accuracies better than 90% and 98% for limited and full view data respectively.

# CHAPTER 1

## INTRODUCTION

### 1.1 Introduction

Electromagnetic fields play an important role in modern life. They have been used in many different devices for many different purposes, such as in wireless communication, heating in the microwave ovens, medical X-ray and tomography. As a result, it has become increasingly important in the good understanding of the electric field and how it interacts with the environment. The propagation of the electric field is governed by a set of differential equations called Maxwell's equations (Maxwell, 2002). Although these equations are simple in itself, the complexity comes from the addition of materials as well as the boundary conditions which prevent the exact solutions for most of the problems in the real life.

As experiments are usually very expensive and significantly time-consuming, numerical simulations have been considered the most viable tool for analysis and optimal design. Noticeably, techniques for electromagnetic computations have been developed considerably in the last two decades due to the availability of high-powered computers. In the past, the main focus of computational electromagnetics had been the development of an efficient solver for the 'direct problems'(Abenius, 2004). These solvers dealt with the solution of Maxwell's equations where all the physical parameters were known. In recent years and due to explosive growth in computational resources,

electromagnetic computation has moved a further step to solve the most interesting and challenging problems, such as inverse problems. In these problems only some of the physical parameters are known, while others can be found by interpreting some of the measurements taken outside.

Electromagnetic inverse and direct scattering problems come in pairs. Hence, in any electromagnetic problem it is necessary to distinguish between the fundamental parts, consisting of the governing equations, and the data, i.e. boundary and initial conditions, sources and physical properties, such as geometry and media. Finding the fields from the governing equations, with given data, is the direct or forward problem. In the inverse problem, the field is partially known, for example from measurements or design objectives, and it is desired to determine the data from which this observed field originates. In particular, the investigation of an object, by measuring the scattered field outside the object, is called ‘inverse scattering’.

The main objective of this research is to develop time-domain inverse scattering algorithm to cope up with the 2-D inverse problem. Therefore, this chapter is devoted to give a brief background of the inverse electromagnetic problem which includes its definition, mathematical challenges, applications and development of inversion algorithms; while the last two sections of the chapter discuss the objectives and outline of the current research.

## 1.2 Inverse Electromagnetic Scattering

Anyong et al. (2001) defined the inverse scattering as the recovery of some inaccessible information from electromagnetic fields measured in the exterior region. The exterior region could be homogenous or inhomogenous, of any dimension, with or without electromagnetic scatterers. In this respect, the information of interest is the location, shape, size, and electrical properties of electromagnetic constitutive parameters. Most of the electromagnetic scattering problem can be considered as an active system where a known incident field is artificially applied to illuminate the inaccessible unknown scatterers to give rise to the scattered field, which is measured at some accessible area. However, such as passive remote sensing in which the scattered electromagnetic fields from the unknown scatterers are not due to such artificially applied incident electromagnetic fields. Usually, the scattered electromagnetic fields are measured over a limited domain of aspect angle, frequency, and polarization and are contaminated by noise and measurement errors.

Electromagnetic inverse scattering is concerned with how one can obtain a large part of information about the surrounding world. Everyday example of electromagnetic inverse scattering is the human vision; from the measurements of scattered light that reaches eye's retinas, the brain constructs a detailed three-dimensional map of the real world. This is a highly automated process, and most of people are not aware of how difficult this problem is. In fact, a large part of the human brain is devoted to such activities.

### **1.2.1 Mathematical Challenges**

The inverse scattering problem is mathematical in nature, and it is more difficult to solve in comparison to the direct problem due to the following challenges.

#### **1.2.1.1 Electromagnetic Scattering**

Studying the inverse scattering problems requires a deep knowledge of the corresponding direct scattering problems (Potthast, 2001). Unfortunately, these studies are still far from perfect. For example, the current understanding of the propagation of waves in complex and random medium is still at infant stage.

#### **1.2.1.2 Non-linearity**

The direct scattering problems are linear in nature, in a sense that for known scatterer the relationship between the incident fields and scattered fields is linear. However, for inverse scattering problems, the most important part is the relation between the scatterer and its response to the incident fields which is inherently non-linear (Colton and Kress, 1992). The non-linearity is caused by the multiple scattering effect due to the presence of the strong scatterer. Therefore, ignoring this non-linear relationship of inverse scattering is considered as lost in the linear approaches of the inverse scattering. The first consequence of this loss is that these approaches can only produce qualitative images rather than quantitative images. The second consequence is that it precludes the use of the linear approaches except in the limiting case of scatterers that are large compared to a wavelength.

### **1.2.1.3 Ill-Posedness**

The mathematical formulation of inverse scattering problems leads to models that are typically ill-posed. According to (Hadamard, 1952), three conditions are found for any mathematical problem to be well-posed: first; when a solution exists; second, when solution is unique; and third, when solution depends continuously on the data. If one of these properties is violated, the problem is called ill-posed. Neither existence nor uniqueness of a solution to an inverse problem is guaranteed. Non-uniqueness is sometimes of advantage, which allows choosing among several strategies for obtaining a desired effect. In non-linear inverse problem applications, exact data does not exist but only data perturbed by noise are available, due to errors in the measurements, or due to inaccuracies of the model itself. Even if their deviations from the exact data are small, algorithms developed for well-posed problems fail in the case of a violation of the third Hadamard condition. In case of the existence of such instability in the data, there should be a protocol that uses regularization methods to replace an ill-posed problem by a family of neighboring well-posed problems (Tikhonov and Arsenin, 1977).

### **1.2.2 Application of Electromagnetic Inverse Problem**

Although, the inverse scattering problem is a relatively new area of electromagnetic, it has gained a lot of attention by researchers and it has been increasingly used by many disciplines into different practical applications. Since the mid-1980, an explosion has been witnessed in the application of electromagnetic inverse problems. Some of these applications in different disciplines are briefly discussed below.

### **1.2.2.1 Military Applications**

Military applications represent one of the most important stimulation for the development of inverse scattering problems due to the success of many inventions, starting by the invention of the radar in World War II used in the detection and identification of hostile and friendly targets. Additionally, when the world moved towards increasing peace military demands on electromagnetic inverse problems, for example, in countries under the threat of landmines as a consequence of early wars, electromagnetic inverse scattering represented the most effective tools to detect and remove these mines; thus preserving human life. Another example is the satellite networks and missile defense systems, which are being built to defend against attacks from hostile countries. Figure 1.1 illustrates one of the latest ways of inverse scattering application to detect the land mines. It is one of humanitarian aerial land mine detection systems designed by the Lawrence Livermore National Laboratory (LLNL) (Pardo Seco, 2008). The system is equipped with an array of ultra-wideband radar sensors and sophisticated subsurface tomography algorithms, both developed by LLNL, that provide exceptional quality subsurface images. These technologies are combined with Hystar, aerial vehicle with unique flight capabilities that permit remote, reusable and safe operation for sensor platforms (Wampler, 2009). Its operation is based on the reflection mode, and it has the ability to penetrate dielectric materials like wood, concrete, and soil and provide high resolution detection of changes in embedded material dielectric and conductivity properties. Moreover, it improves the safety to personal and equipments in the field.



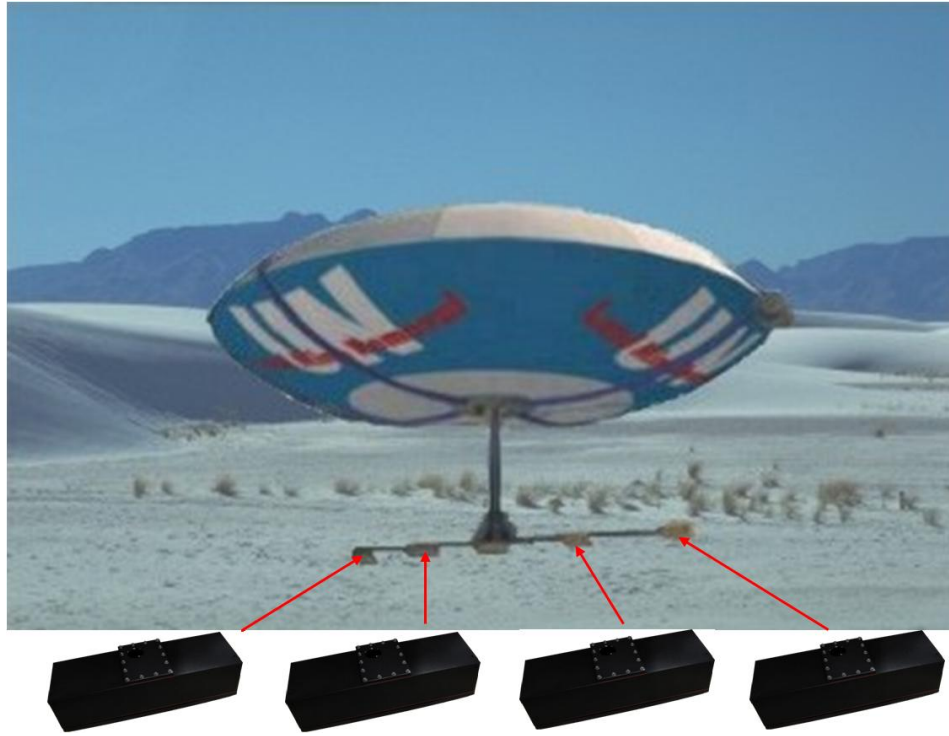


Figure 1.1 Latest system for land mines detection (Wampler, 2009).

### 1.2.2.2 Medical Applications

Inverse scattering application has also its implications on the medical field in which today hospitals and medical centers rely heavily on medical devices that work on the basis of inverse electromagnetic scattering for diagnostic, detection and treatment purposes. The starting point of the inverse scattering medical application revolution was the invention of X-ray by Roentgen (Shastri, 2008), and it has continued through the invention of X-ray computer assisted tomography " CAT " by Hounsfield in 1972 (Suetens, 2002), which replaced the conventional x-ray machines in many hospitals. Figure 1.2 shows an example of a CAT machine. More recently, some CAT machines have been replaced by more advanced nuclear magnetic resonance imaging machines for accurate diagnosis (D'Haenen et al., 2002).



Figure 1.2 Shows the CAT machine commonly used by hospitals (IMAGING, 2009)

### 1.2.2.3 Industrial Applications

Electromagnetic inverse scattering is of the great commercial value for industries, for example, oil companies; in detecting the location of oil in the subsurface (Friedman, 1998). Another example is the controlling and monitoring of the oil flow in pipelines between production fields and consumption or export places by using tomography (see Figure 1.3). This is almost done with significant computation cost performed by the oil companies. In fact, much of the recent resurgence in the oil industry is due to improvements in mathematical algorithms that allow scientists to see through salt layers to detect the oil-bearing strata below.

Ground penetrating radar, another example, is a high commercial solution for non-destructive testing that produces cross section profile or record of subsurface features without any drilling, digging or probing. Commercial aviation industry has significantly benefited from the applications of the electromagnetic inverse problem, for example in security checking where it is mandatory for all passengers to pass this check before boarding the aircraft, including metal detectors and others. Other industries have taken a lot of advantages from the application of electromagnetic inverse problems including nuclear energy and food construction.

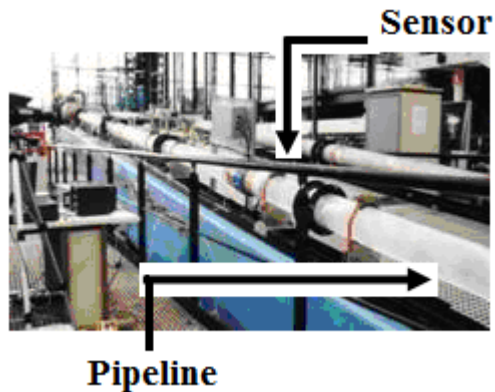


Figure 1.3 Capacitance type of process tomography flow sensor (Xie et al., 1992)

#### 1.2.2.4 Scientific Applications

Electromagnetic inverse problems have been enormously influential in the advancements of natural science and of great advance in science and technology. Their solutions have provided significant amount of information, such as the discovery of the structure of DNA through X-ray diffraction problem (Krude, 2004), and the structure of the atom and its constituents from studies on scattering phenomena of particles-bombarded materials. One example of these machines that can be used in this type of

problem is called X-ray diffraction equipment shown in Figure 1.4. Over years, the electromagnetic inverse problem has played an important tool in many scientific areas such as archaeology, seismology, geophysics, optics, material science, and meteorology (Banhart, 2008).



Figure 1.4 X-ray Diffraction Equipment Used in Scientific Applications (EQUIPMENT, 2009)

### 1.2.3 Development of Inversion Algorithms

For the electromagnetic inverse problems, the main research areas are ordered according to their importance in real life applications: first, developing new inversion algorithms; second, finding new applications for the existing algorithms; and third, building a prototype and commercializing it. The core of the current research in this thesis focuses primarily on the first research area, i.e. developing relatively new

inversion algorithms. Therefore, the remaining part of this section discusses briefly an introduction on the development of the inversion algorithms.

### **1.2.3.1 Linearized Inversion Algorithms**

These inversion algorithms represent the early attempts for solving inverse scattering problems by making some approximations to ensure the linearity of these problems, such as the Born approximation (Vegetti and Aks, 1979), the Rytov approximation (Cairns and Wolf, 1990) and Ray approximation (Kang and Griffiths, 1993). Despite the lack of success in retaining the non-linear nature of the inverse scattering problems, inversion algorithms succeeded in resolving some of these problems through some restrictions. One example of such a restriction is an assumption of the weakly scattered object. The most prominent inversion algorithms classed under this type include layer stripping algorithm (Marsili et al., 1992), the Born approximation algorithm, the Rytov approximation algorithm and linear diffraction algorithm. However, the approximations made to obtain these inversion algorithms make their application limited and cannot be used for wide range of applications.

### **1.2.3.2 Non-linear Inversion Algorithms**

As mentioned previously, the non-linearity is one of the main features of the inverse scattering problems. Nevertheless, developers of the linear inversion algorithms practically underestimate this important aspect, making such algorithms limited in application. On the other hand, the non-linear inversion algorithms represent the correct way to solve these kinds of problems by retaining their non-linearity nature. Most of the

non-linear algorithms are mathematically difficult and computationally expensive due to their iterative nature; while on the other hand they are more versatile and accurate, making them more attractive for practical applications.

In this class of algorithms, the inverse scattering problems are reformulated as optimization problems. These algorithms are classified according to the optimization techniques used, either the local inversion algorithms or global inversion algorithms. The local inversion algorithms are gradient based algorithms and include the distorted born iterative technique (Lu et al., 1996), Newton-Kantorovich algorithm (Roger, 1981b), conjugate gradient method (Harada et al., 1995), and the local shape function method (Weedon and Chew, 1993). The local inversion algorithms are less in computational cost in comparison to the global inversion algorithms, but they mainly depend on the initial guess. According to this guess, they can be converged, fall in local minimum or diverged. On the other hand, the global inversion algorithms are costly in computation but are more versatile and accurate. They have a strong ability in searching, and may include the Genetic algorithm (Chiu and Liu, 1996), neural network (Rekanos, 200b) and simulating annealing (Garnero et al., 1991), making these algorithms in general of stochastic base.

Another class of non-linear algorithms has been developed called hybrid algorithm (Mathias et al., 1994). This algorithm attempts to reduce the computational cost of global inversion algorithms as well as to keep their ability of good searching process, including high precision in finding global minimum. This process is done through a combination of local and global inversion algorithms by, firstly applying the global

inversion algorithm to obtain a good initial guess for local algorithms, and secondly applying the local to complete the searching processes to find the global solution. Common practice for this approach is to use pre-defined threshold. Once the global inversion algorithm exceeds the pre-defined threshold, the searching process is transferred to the local inversion algorithm. One famous example of these types of algorithms is the combination of the real coded genetic algorithm and Newton Kantorovich algorithm (Qing and Lee, 2000.).

In the current research, a non-linear inversion algorithm, based on the local inversion methods, has been developed. Also a special case solution of this algorithm has been examined, on the basis of Born approximation.

### **1.3 Thesis Objectives**

#### **1.3.1 General Objective**

The overall objective of this thesis is to develop linear and non-linear inversion algorithms in the time-domain, leading to an improvement of modeling and image reconstruction of soft field imaging modalities.

#### **1.3.2 Specific Objectives**

Five specific objectives of this study are listed as follows:

- i. To investigate the validity of using the finite difference time-domain method for solving two dimensional forward electromagnetic problems.

- ii. To investigate the efficiency of the two most common absorbing boundary conditions used to truncate the outgoing electromagnetic wave from return to the computation domain. They are Mur's and PML absorbing boundary conditions.
- iii. To develop both linear and non-linear inversion algorithms in time-domain for image reconstruction of microwave imaging using ultra wide band sensors.
- iv. To validate both proposed algorithms: linear and non-linear inversion algorithms using simulated data generated from limited and full view geometries.
- v. To validate the algorithm using real data generated from experimental setup, simulating limited and full view geometries.

#### **1.4 Thesis Outlines**

The thesis is composed of six chapters. Chapter 1 deals with the development of linear and non-linear time-domain inversion algorithms that can be applied for medical imaging as well as nondestructive testing. In Chapter 2, a review of tomography science including its definition, history, main groups, mathematical basis for the main types of tomography, non-linear inverse scattering algorithms, including the current state of art is introduced. The discussion then is followed by highlighting the optimization methods, and elaboration on the proposed algorithm developed in this research. Chapter 3 addresses the problem in further details on the algorithm formulation, the conditions for solutions and finally proposing optimization methods for problem solutions.



Experimental setup is discussed in Chapter 4 together with the finite difference time-domain method as a preferred numerical method for both forward and inverse problem solutions. The overall results including both simulated and experimental results are presented and discussed in details in Chapter 5 in numerical and graphical features. Finally, Chapter 6 comes to conclude the findings of this research and projects future works and development endeavors for future researchers and interested workers.

## **CHAPTER 2**

### **LITERATURE REVIEW**

#### **2.1 Introduction**

Tomography comes from two Greek words, the first one is “tomo“ means sectional and the second is “graphy” means representation (Kak et al., 1988). Thus, a tomographic image is a cross sectional image of an object. Today, tomography refers to a procedure to collect data about the internal structure of an object and then mathematically generate an image of some otherwise hidden property of the object. On the other hand, tomography is a general word for all imaging modalities includes electromagnetic, acoustic and nuclear imaging.

#### **2.2 Tomography History**

In this section, the historical development of tomographic imaging is discussed. Since it cannot cover all types of tomography imaging, the following discussion will concentrate mainly on some types of tomography that have high impact on medical field. The tomography in general can be classified into ionizing and non ionizing techniques (Xu and Eckerman, 2009). The distinction between ionizing and non ionizing radiation is essentially important in distinguishing the effect of both on biological systems. Ionizing radiation can cause serious irreversible chemical changes as it breaks chemical bonds .This can potentially cause biological and health defect in living system. As a result, exposure to this kind of radiation should be limited. Non-ionizing radiation, in general can only cause tissue heating; making these techniques having an advantage of being safer in comparison to ionizing techniques (Lim, 2003). To give a clear picture

of those classes, one example is selected from each class. These examples which are discussed here include: computed tomography (CT), belonging to the family of ionizing techniques; and ultrasound tomography, belonging to the family of non-ionizing techniques.

### **2.2.1 Computed Tomography**

A considerable number of medical equipments rely on tomography imaging systems, like computed tomography, ultrasound, microwave and others. Since hundred and twenty years ago, the only way to look into the patients' body was via invasive procedures. Few years later, Wilhelm Rontgen discovered X-ray in 1895. That invention opened the door for the first medical instrument by which the specialist was able to look into the patients' body via non-invasive procedures, and called later as x-ray tomography. Soon, this imaging modality had become an important tool in medical diagnosis. Since then the first revolution of tomography had started and this continued through establishing its mathematical foundation in 1917 by Johan Radon, an Australian mathematician. He put the mathematical foundation for tomography showing that the reconstruction from projection is possible (Deans, 1983). This concept was first applied by R.N. Bracewell to reconstruct a map of solar microwave emission from series of radiation measurements across the solar surface (Bracewell, 2003). Later, several Russian papers have accurately formulated reconstruction as an inverse Radon transform (Hsieh, 2003).

The reconstruction of images from projections was attempted as early as 1940 without the use of the modern computer technology. In 1940, Gabriel Frank was able to describe the basic idea of modern tomography including such concepts as Sinograms (i.e. representation of measurement data as linear samples versus view samples) and optical back projection (Hsieh, 2003). In 1956, Allan M. Cormack conducted experiments on reconstructive tomography in medical applications. He reconstructed attenuation coefficients of tissues to improve the accuracy of radiation treatment, which led to the development of a mathematical theory for image reconstruction by introducing the Fourier transform in the reconstruction algorithms. However, due to the difficulty of calculations, his work was not recognized at the time. The first clinical CT scanner was developed in 1967 by Godfrey N. Hounsfield at the Central Research Laboratories of EMI, Ltd., in England. When he was investigating pattern recognition techniques, he concluded that X-ray measurements taken through a body from different directions would allow the reconstruction of its internal structure. Due to the low-intensity of the gamma source, it took 9 days to complete the data acquisition and construct the image including the computation of 28,000 simultaneous equations within 21 hours (Hsieh, 2003). After further refinement of the data acquisition, images were constructed in less than 5 minutes. This led to the installation of the first clinical CT device at Atkinson-Morley Hospital in September 1971. A month later, the first patient with a large cyst was scanned, and the pathology was confirmed from the image. In 1979, Cormack and Hounsfield shared the Nobel Prize for their contributions to the development of first generation computed tomography (Hsieh, 2003). Since then, research has started the second revolution which led to tremendous advancements of developing the second, third, fourth and fifth generations of computed tomography.

### **2.2.2 Ultrasound Tomography**

Ultrasound tomography, on the other hand, is an alternative imaging modality, and the main advantage of it over the other modalities like CT is the use of non-ionizing source, which makes it safer compared to other modalities. The first motivation for using ultrasound for tomography purpose was the sinking of Titanic on its maiden voyage in 1912. However, it was not employed for medical purposes until the beginning of the 1940s when Dr. Karl Dussik, a psychiatrist from Austria, was the first specialist attended to use ultrasound in medical diagnosis in 1942 (Peter, 2009). He faced some difficulties in the process due to the absorption of the most ultrasound energy by the bones of the skull. After intensive efforts done by several physicists, mechanics, engineers, electricians and biologists in collaboration with doctors and computer programmers, researchers and government support, ultrasound diagnostic began to take place in nerves, heart and eyes clinics. This effort led to development of A-mode waves of limited use compared to B-mode wave, which have more ability to penetrate different types of tissues. In 1951, Douglas Howry, a radiologist from University of Colorado, and Joseph Holmes in collaboration with John Reid and John Wild, developed the first 2D B-mode linear compound scanner (Howry et al., 1954). Since then, the production of the B-mode based instruments continued, but their main limitations were known to be for their large size and the preparation needs to insert the patient in water either fully or partially for long hours before scanning. These limitations made these instruments impractical for clinical usage.

In mid 1960s, the world witnessed the development of these scanning devices to become more sensitive and smaller and easier in testing process. The late 1960s and early 1970s were referred to as the sonic boom, according to John Baker (Beth, 2008). During this period, 2D echo was introduced by Klaus Bom. In 1966, Don Baker, Dennis Watkins, and John Reid developed pulsed Doppler (Beth, 2008), which enabled the detection of blood flow from different depths in the heart.

The real revolution of ultrasound has started by the appearance of the first real-time ultrasound in the early 1980s. With this revolution, the identification of actual life, actions and heartbeats of fetal in the mother womb became possible. The first effective system based on real time ultrasound was built in 1985 in German. Since then, in the eighties and early nineties, the field of competition between companies began producing the most accurate real time instruments with the clearest images, which led to a great progress in the production of 2-D real time ultrasound systems made by these companies.

Moreover, as the result of advancement in science and computation resources, it was evident that 2-D ultrasound systems, in spite of their previous profound success, need to be upgraded to incorporate the new scientists' perspective of the third dimension. The late 1980s represented the early appearance of 3-D ultrasound systems (Beth, 2008). However, one of the most important problems experienced by the early prototype of these systems is the length of time taken to produce a cross section, and sometimes each cross section took up to ten minutes. The development of three-dimensional ultrasound systems continued until an intensive research about the four-dimensional systems started in London 1996. This led to the emergence of the idea of real time three-dimensional

systems where the fourth dimension is the time dimension. These systems allowed for producing real images in a practical way that was unachievable without the significant development of computer science and the substantial progress in computational resources.

The advantages of microwave and ultrasound imaging over conventional imaging are numerous. First, they include the relatively low health hazard of non-ionizing, low power of sources. Second, they are able to image physiological properties of tissue and organ. Third, the likely cost competitiveness of the imaging equipment makes such modern imaging modalities favorably desired. Moreover, a key promising future of microwave imaging is in the application of breast cancer detection, where thermal and ionizing radiations, found in the conventional imaging systems, are readily avoided. In addition, the contrast in dielectric properties between malignant and background fat tissue can easily help in identifying cancer tumors (Lazebnik and Magliocco, 2007).

Tomography in general has found tremendous success in several fields such as medical imaging (Bolomey et al., 1984, Bolomey et al., 1992, Jofre et al., 1990, Joisel et al., 1999, Semenov et al., 1996a, Semenov et al., 1996b, Wael et al., 2004), nondestructive testing (Hui et al., 2006, Mudanyal et al., 2008, Pastorino et al., 2001, Saleh and Qaddoumi, 2003), geophysics (Molyneux and Witten, 1993, Nolet, 1987) and environmental application (D'Antona and Rocca, 2004, Todd et al., 2001).

### **2.3 Soft Field vs. Hard Field Systems**

Different sensors can be used for tomographic imaging and each one can be sensitive to certain feature. Therefore, the parameter or characteristic to be imaged is determined by the type of sensor chosen. Capacitance sensors, for example, are sensitive to the dielectric constant of the object, while gamma-rays and X-rays are sensitive to density (Lim, 2003). As a result, there are various tomographic sensing systems available. Generally, such systems may be divided into two groups; soft field and hard field systems. The reason for this grouping is to know whether a distribution of system parameter has an influence on the field sensor. This knowledge will affect later on the choice of the inversion algorithm and overall design of the tomography system with the consequent effects on the cost of the system (Plaskowski, 1995).

Soft field systems include electrical tomography, (capacitance, resistance, and impedance); electromagnetic imaging, (microwave and radar); nuclear magnetic resonance imaging (NMRI); optical tomography; and ultra sound imaging. On the other hand, the hard field systems include x-ray; gamma-ray; and neutrons. A hard-field sensor is equally sensitive to the parameter it measures in all positions throughout the measurement volume. Its sensitivity is also independent of the distribution of the measured parameters inside and outside this measurement region (Plaskowski, 1995). For a soft-field sensor, on the other hand, sensitivity to the measured parameter depends on the position in the measurement volume, as well as on the distribution of parameters inside and outside this region. For this reason, soft field system is more complex because their measurements produce sets of non-linear equations making the inversion more



difficult to implement and produces low resolution images, whereas hard field systems produce sets of linear equation making the inversion simple and produces high resolution images (Plaskowski, 1995). On the other hand, the main reasons have restricted the hard field application in some practical situation are the high cost and the use of ionizing radiations. The former forbids their widespread use, especially in developing countries while the exposure of the later is damaging to some materials like human tissues, and the harmful effects are cumulative.

Soft field systems are attractive alternative modalities for those materials like human tissues. Among them the most promising imaging modality is the electromagnetic imaging including microwave, its system cost is a small fraction of the cost of hard field like an X-ray system, making it affordable for widespread use. Also, the system poses no safety hazards, and the potential is significant for detecting very small objects with high resolution.

There are two key issues to address when implementing a microwave imaging system. One is the hardware problem including the increase of the signal to noise ratio in the system and to assure that the system has a large dynamic range. The importance of this is closely related to the fact that the scattered signal is often very weak in comparison to the transmitted signal. This implies that any noise in the system will have a large impact on the image quality and that the system must be able to distinguish even small differences in the received signals, and the other issue is the way to obtain the maximum amount of information from microwave measurements. The later was the target of this research, and it was overcome by applying the time-domain inverse

scattering techniques. This technique is known to utilize the full waveform inversions based on approximate solution of the Maxwell's equation.

The remaining sections of this chapter deals with the mathematical basis of tomography, both non diffraction and diffraction sources, the evolution of the inverse scattering algorithms including the current state of art, and finally a summary of optimization methods available including their advantages and limitations.

#### **2.4 Non-Diffraction Tomography**

Non-diffracting tomography refers to imaging with non-diffracting sources like hard field sensors. Hard field sensors are classified under this category because they are equally sensitive to the parameter they measure in all positions throughout the measurement volume and their sensitivities are also independent of the distribution of the measured parameters inside and outside this measurement region. This property makes the fields propagate in straight lines without any reflections or refractions. As a result, the projections for these sensors are a set of measurements of the integrated values of some parameters of the object where the integrations are taken along straight lines through the object and being referred to as line integrals. A typical example of these sensors is the attenuation of x-rays as they propagate through biological tissue. In this case, the object is modeled as a two-dimensional (or three-dimensional) distribution of the x-ray attenuation constant and a line integral represents the total attenuation suffered by a beam of x-rays as it travels in a straight line through the object.